Efficiency of US Tissue Perfusion Estimators

MinWoo Kim, Craig K. Abbey, and Michael F. Insana, *Fellow, IEEE*

Abstract—We measure the detection and discrimination efficiencies of conventional power-Doppler estimation of perfusion without contrast enhancement. The measurements are made in a phantom with known blood-mimicking fluid flow rates in the presence of clutter and noise. Efficiency is measured by comparing functions of the areas under the ROC curve for Doppler estimators with that of the ideal discriminator, for which we estimate the temporal covariance matrix from echo data. Principal components analysis is examined as a technique for increasing the accuracy of covariance matrices estimated from echo data. We find that Doppler estimators are less than 50% efficient at directed perfusion detection between 0.1 and 2.0 ml/min per 2 cm^2 flow area. The efficiency was 20-40% for the task of discriminating between two perfusion rates in the same range. We conclude that there are reasons to search for more efficient perfusion estimators, one that incorporates covariance matrix information, that could significantly enhance the utility of Doppler ultrasound without contrast enhancement.

Index Terms—Ideal discriminator, pulsed Doppler ultrasound, ROC analysis, tumor perfusion

I. INTRODUCTION

One of the many capabilities of ultrasonic imaging is the ability to assess blood flow in tissues using pulsed-Doppler techniques. Unlike color-Doppler imaging that derives its signal from coherent directional motion, power-Doppler methods [1] measure decorrelation of the backscatter signal over time at fixed points. Power Doppler methods are applied medically to evaluate vascular flow and detect blood perfusion through capillary networks [2]–[4].

When assessing slow flow in the microvasculature, the blood and clutter components of the Doppler frequency spectrum overlap significantly. Coupling that overlap with the weak backscattering properties of red blood cells (RBCs), it can be challenging to use power Doppler methods to detect neovasculature without contrast enhancement [5]. Blood-born gaseous agents have been successful at boosting the blood component of the echo signal, which leads to improved separability of RBC motion from tissue clutter and acquisition noise [6]. However, contrast agents increase exam cost and complexity [7]. Non-contrast power Doppler methods would be ideal for noninvasive perfusion imaging provided the blood echoes can be reliably detected and separated from clutter and noise components of the echo signal.

In this report, we examine the ideal (ID) discriminator of ultrasonically-detected blood-perfusion states. This statistical discriminant function leverages properties of the tempo-ral covariance matrix of RF echo signals to describe echo decorrelation within a scattering region caused by scatterer motion and noise. The ideal discriminator fully incorporates statistical information about the random object scatterers into a scalar test statistic that maximizes the area under the receiver operating characteristic (ROC) curve [8], or AUC, thus maximizing classification performance [9] [10]. Provided scattering is an incoherent Gaussian process, all anatomical and flow information is found within the covariance matrix of the object scatterers. The object function covariance matrix is simply related to that for the pulse-echo measurements using linear systems [11].

Heimdal and Torp [12] used a statistical discriminant function as a new color-Doppler estimator in a manner similar to the analysis described below. Later Hovda et al. [13] also applied statistical estimators in a technique they called knowledge-based imaging. They both found the statistical approach to flow estimation can be very sensitive to flow, but it requires knowledge of the covariance matrices for all possible flow conditions. Our goal in this report is to use statistical estimators to assess the efficiency of standard power Doppler methods.

The temporal covariance matrix for an imaging experiment is a combination of pulse properties, scatterer echogenicity, and scatterer movement. When these properties are known, as they can be in phantom measurements, the covariance matrix for specific flow conditions can be estimated from echo samples. Then the ideal discriminator described in this paper can be computed and its performance compared with standard methods to estimate flow discrimination efficiency. Efficiency quantifies the fraction of available task information being used by the estimator. Traditional power-Doppler methods are suboptimal discriminators because they fail to incorporate all of the specific information about the interaction between pulse and scatterer motion interactions. This information is specific to each perfusion event but unknown during clinical studies.

The first step in our approach is to estimate the temporal covariance matrix of RF echo-data measurements obtained from a perfusion phantom. We explore how the amount of RF echo data used for ensemble averaging influences covariance estimates. For this aspect of the study, we apply principal-components analysis (PCA) [14] to the echo covariance matrix to separate blood echoes from tissue clutter and acquisition noise [15] in an attempt to reduce the amount of echo data required to accurately estimate the covariance matrix.

We then show that power Doppler estimates that employ FIR clutter filters can be expressed in a manner analogous to the ID test statistic. ROC curves are generated for comparisons of both methods. From perfusion phantom data, we estimate ROC curves for discriminating between pairs of flow states using conventional power Doppler methods. These results

MinWoo Kim is with the Department of Electrical and Computer Engineering, University of Illinois at Urbana-Champaign (mkim180@illinois.edu).

Craig K. Abbey is with Department of Psychological and Brain Sciences, University of California Santa Barbara (craig.abbey@psych.ucsb.edu).

Michael F. Insana is with the Departments of Bioengineering, ECE and the Beckman Institute for Advanced Science and Technology, University of Illinois at Urbana-Champaign (mfi@illinois.edu).
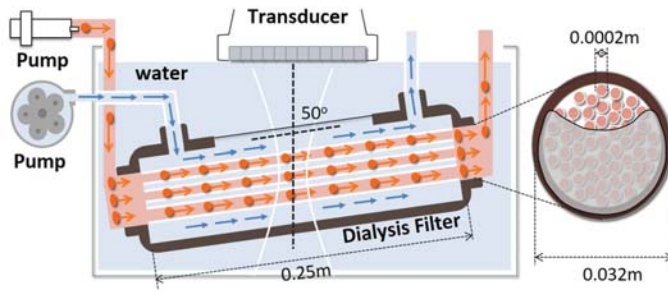
Fig. 1. A dialyzer cartridge was used to mimic blood perfusion in a clutter and noise environment. An ultrasonic linear array scans the cartridge to acquire echo data in spectral Doppler mode. Perfusion rates are controlled by a syringe pump infusing either water or blood-mimicking fluid through the fibers while a peristaltic pump circulates the water surrounding the fibers to simulate clutter. As shown, blood-mimicking fluid flow was limited to a cross-section of fibers about 25% ($\sim$2 cm^2) of the total area.

are compared to the ID results to estimate the efficiency of conventional methods. Finally, we show how the binary discrimination task may be extended to more general flow conditions in a way that illustrates how inefficiency reduces the visibility of flow in power Doppler images of the phantom.

By estimating efficiency, we hope to motivate the need for new perfusion estimation methods by quantifying the potential improvements that could result. The analysis presented applies to any experimental approach to perfusion imaging using pulse-echo ultrasound.

II. METHODS

A. Flow Phantom

Ultrasonic measurements were made using the perfusion phantom illustrated in Fig. 1. The critical unit was a dialyzer cartridge consisting of a bundle of hundreds of 0.2-mm inner-diameter polysulfone fibers (B. Braun Medical Inc., Allentown, PA USA). Using a programmable syringe pump connected to the cartridge, we steadily infused in a closed loop through the fibers either pure water for the control state or blood-mimicking fluid (CIRS, Norfork, USA) for the test state. In this way we simulated spatially-directed blood perfusion in the range of 0.0 - 2.0 ml/min over a cross-sectional area approximately 2 cm^2 [16]. In addition to intra-fiber infusion, a second set of cartridge connections allowed water to be pulsed into the cartridge outside the fibers. Connecting a 1 Hz peristaltic pump in this way, we simulated clutter from cardiac motion. A portion of the protective plastic case was removed to provide an acoustic window, and then the entire cartridge was submerged in degassed water at room temperature.

We limited flow to just the most proximal 2 cm^2 of the cross sectional fiber area so that net flows $\leq$2 ml/min provided representative scatterer velocities within the fibers. We note that the density (1.24 g/cm^3) and longitudinal sound speed (2260 m/s) of the polysulfone fibers present a strong impedance mismatch with the surrounding fluids, which reduces sound penetration and echo SNR. However the ideal detector is limited by echo SNR in the same way as other estimation methods, so that discrimination efficiencies will be relatively

unaffected, even if this represents a somewhat more difficult environment for perfusion estimation.

B. Signal Model

All modeling and analysis were conducted in MATLAB . In a spectral-Doppler acquisition, a single line of sight (Fig. 1) is repeatedly probed with N' narrow-band pulses as M' range echoes are recorded after each pulse transmission. The result is $M' \times N'$ matrix $\mathbf{X}'$ with elements $X'[m,n]$. Two examples are shown as gray-scale images at the top of Fig. 2.

Column vectors of $\mathbf{X}'$ describe temporal sampling along a fixed transducer line of site; each vector is the RF echo signal from the nth pulse along the "fast-time" axis, $\mathbf{x}_n$ with elements $x_n[m]$ and $0 \leq m \leq M'-1$. Row vectors $\mathbf{x}_m$ are echoes along the "slow-time" axis where echo signal samples are $x_m[n]$ for $0 \leq n \leq N'-1$. Integer index m also indicates the distance z from the transducer surface (depth) via $z[m] = z_0 + cmT'/2$, where z_0 is the distance at which recording begins, c is the compressional wave speed, and T' is the fast-time sampling interval. The time interval between pulse transmissions (and slow-time samples) is T, $1/T$ is the pulse repetition frequency, and $T \geq M'T'$. Since the fast-time axis also corresponds to depth, we may consider $\mathbf{X}'$ as composed of echoes recorded at M' depths each from N' pulses along the slow time axis.

The temporal covariance matrix for zero-mean echo signals recorded at depth $z[m]$ is the expected value of the outer product of the mth row vector in $\mathbf{X}'$, i.e., $\mathbf{\Sigma}_x = E(\mathbf{x}_m \mathbf{x}_m^{\mathsf{T}})$, where superscript T indicates vector transpose. We assume the standard physical model of blood flow in Doppler ultrasound, where there are three stochastic sources contributing to $\mathbf{\Sigma}_x$ [9], [15], [17]–[19], and each source is assumed to be an independent zero-mean multivariate normal random process. The three covariance sources are tissue scattering represented by matrix $\mathbf{C}$ (for clutter), blood scattering by matrix $\mathbf{B}$, and acquisition noise by matrix $\mathbf{E} = \sigma_e^2 \mathbf{I}$. The quantity σ_e^2 is the noise variance and $\mathbf{I}$ is an identity matrix. Unlike $\mathbf{E}$, matrices $\mathbf{C}$ and $\mathbf{B}$ are not diagonal, representing the fact that clutter and blood signals persist to some extent through time. They contribute to $\mathbf{\Sigma}_x$ through the filter of instrumentation,

$$\mathbf{\Sigma}_x = \mathbf{\Sigma}_c + \mathbf{\Sigma}_b + \mathbf{E} = \mathbf{HCH}^{\mathsf{T}} + \mathbf{HBH}^{\mathsf{T}} + \sigma_e^2 \mathbf{I}, \quad (1)$$

where $\mathbf{H}$ is the measurement-system matrix. In this model, all tissue and blood information is contained in $\mathbf{\Sigma}_x$.

In practice, we select an $M \times N$ subset of $\mathbf{X}'$ to form the smaller echo matrix $\mathbf{X}$, where $M \leq M'$ and $N \leq N'$. We then assume there may be a non-zero mean and that the signal are ergodic, where spatial averaging is used in place of ensemble averaging to estimate $\mathbf{\Sigma}_x$. For $M \times N$ echo matrix $\mathbf{X}$, the approximation is the $N \times N$ covariance

$$\mathbf{\Sigma}_x \simeq \frac{1}{M-1}(\mathbf{X} - \overline{\overline{x}})^{\mathsf{T}}(\mathbf{X} - \overline{\overline{x}}), \quad (2)$$

$$\text{with mean} \quad \overline{\overline{x}} = \frac{1}{MN}\sum_{m=0}^{M-1}\sum_{n=0}^{N-1} X[m,n].$$

Ergodicity is possible when the impulse-response function is shift invariant and the contributing sources are stationary for all M rows of $\mathbf{X}$.

If more data are desired for averaging to improve the estimate of Eq. (2), the N' samples in $\mathbf{X}'$ may be partitioned to augment the number of rows. For example, if we recorded $N' = 1000$ pulses at $M' = 100$ depths (total of 1.54 s at 650 Hz PRF), each row could be partitioned and rearranged into five 200-pulse packets to form a 500×200 matrix $\mathbf{X}$, yielding covariance matrices of size 200×200.

C. Ideal Discriminator Approach to Perfusion Estimation

Assuming the covariance matrices can be accurately measured, consider a measurement vector $\mathbf{x}$ (subscript m is understood). Its specific properties are unknown except that it was recorded from one of two possible perfusion states that we label 0 or 1. Echo signals from the two states are both multivariate-normal zero-mean processes,

$$\mathbf{x} \sim \begin{cases} MVN(\mathbf{0}, \boldsymbol{\Sigma}_{x|0}) & \text{for perfusion state 0} \\ MVN(\mathbf{0}, \boldsymbol{\Sigma}_{x|1}) & \text{for perfusion state 1} \end{cases} , \quad (3)$$

where $\boldsymbol{\Sigma}_{x|0} = \boldsymbol{\Sigma}_c + \boldsymbol{\Sigma}_{b_0} + \mathbf{E}$ and $\boldsymbol{\Sigma}_{x|1} = \boldsymbol{\Sigma}_c + \boldsymbol{\Sigma}_{b_1} + \mathbf{E}$. That is, $\boldsymbol{\Sigma}_{x|i}$ are $\boldsymbol{\Sigma}_x$ measured for the ith state, where $i = 0$ or 1. The only difference between these two echo-signal distributions is the perfusion rate via $\boldsymbol{\Sigma}_{b_i}$.

The classification task is to decide to which state $\mathbf{x}$ belongs. That task is optimally achieved by the likelihood ratio test [20] given by the ratio of echo probability density functions conditioned on the two states,

$$\ell(\mathbf{x}) = \ln \frac{p(\mathbf{x}|1)}{p(\mathbf{x}|0)} \sim \frac{1}{2}\mathbf{x}^{\mathsf{T}}(\boldsymbol{\Sigma}_{x|0}^{-1} - \boldsymbol{\Sigma}_{x|1}^{-1})\mathbf{x} = \mathbf{x}^{\mathsf{T}}\mathbf{Q}\mathbf{x} . \quad (4)$$

The symbol $\sim$ is used to indicate terms independent of $\mathbf{x}$ are discarded since they do not influence classification performance [11]. Scalar $\ell(\mathbf{x})$ is the test statistic for the ideal discriminator, a quadratic function of testing-data vector $\mathbf{x}$. For convenience, we define the difference between inverse covariances for the two states by the matrix

$$\mathbf{Q} = \boldsymbol{\Sigma}_{x|0}^{-1} - \boldsymbol{\Sigma}_{x|1}^{-1} . \quad (5)$$

In the following, we refer to echo data recorded for estimating $\boldsymbol{\Sigma}_x$ as *training data*. Alternatively the echo data indicated by $\mathbf{x}$ in Eq. (4) are referred to as *testing data*. We train and test on different sets. $\boldsymbol{\Sigma}_x$ are estimated using Eq. (2) and training data. These matrices are nonsingular because of the presence of acquisition noise; their inverses exist as long as there are more samples than degrees of freedom. $\boldsymbol{\Sigma}_x$ and $\mathbf{Q}$ estimations are described in Section II-D and illustrated in Fig. 2.

Decisions based on test vector $\mathbf{x}$ for which $\ell(\mathbf{x})$ has been estimated are expressed as

$$D(\mathbf{x}) = \text{step}(\ell(\mathbf{x}) - \tau) , \quad (6)$$

indicating the decision is state 0 when $\ell < \tau$ and state 1 when $\ell \geq \tau$ for threshold τ. For example, $\ell(\mathbf{x}|1)$ is correctly classified when $D(\mathbf{x}) = 1$ and incorrectly classified when $D(\mathbf{x}) = 0$. To measure discrimination performance, we consider all possible threshold values as shown in Section II-G.
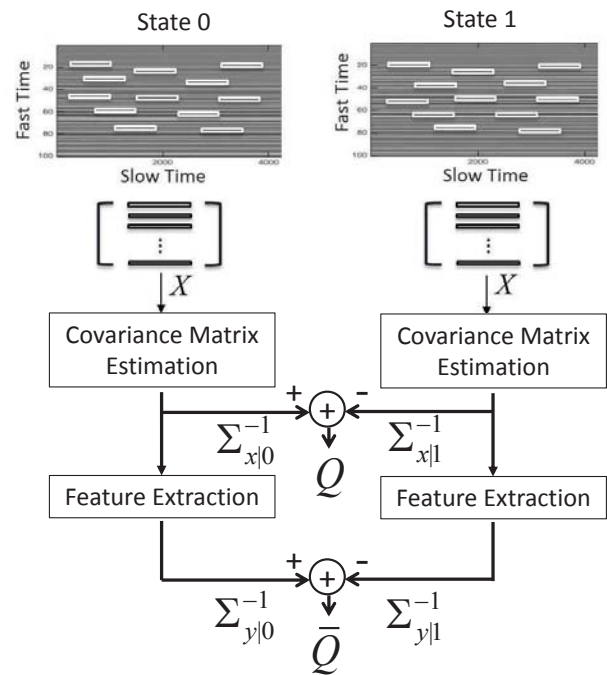

Fig. 2. Illustration of the procedure for generating data matrices $\mathbf{X}$ and covariance matrices $\boldsymbol{\Sigma}_{x|i}$. From covariance matrix inverses, $\mathbf{Q}$ are formed (Eq. (5)) and $\bar{\mathbf{Q}}$ (Eq. (14) in II-H). Echo vectors randomly selected from within $\mathbf{X}'$ (i.e., the small white rectangles in grayscale images at top) are used to form $\mathbf{X}$.

D. Estimating $\boldsymbol{\Sigma}_{x|i}$ and $\mathbf{Q}$

The top of Fig. 2 illustrates the process of randomly selecting data vectors for $\mathbf{X}$ to estimate $\boldsymbol{\Sigma}_x$. In this example, we recorded 3250 (650/s $\times$ 5 s) RF echo signal segments for a fixed-position 2-mm range gate (2 mm$\times$ 20 samples/μs)/(0.77 mm/μs)=52 samples) near the transmit focus of the transducer. Throughout each 52×3250 matrix $\mathbf{X}'$, (grayscale images at top of Fig. 2), we assume the system response is linear time-invariant and the random processes associated with the three sources are wide-sense stationary. We then randomly select packets to form data sub-matrix $\mathbf{X}$. The length and number of packets selected depend on the experiment.

E. Standard Approaches to Perfusion Estimation

We can express standard power Doppler estimation using an expression similar to Eq. (4) as follows for a single test vector $\mathbf{x}$. Techniques that apply a Fourier-domain wall filter to minimize clutter can be written as

$$\bar{\ell} = (\mathbf{F}\mathbf{x})^{\mathsf{T}}(\mathbf{F}\mathbf{x}) = \mathbf{x}^{\mathsf{T}}\mathbf{Q}_{PD}\mathbf{x} . \quad (7)$$

$\mathbf{F}$ is a circulant $N \times N$ matrix that defines a high-pass filter. We define $\mathbf{Q}_{PD} \triangleq \mathbf{F}^{\mathsf{T}}\mathbf{F}$, which is different from $\mathbf{Q}$ that involves covariance matrices in Eq. 4. For example, a DC-cancellation filter is

$$\mathbf{Q}_{PD} = \mathbf{I} - \frac{1}{N}\mathbf{1} , \quad (8)$$

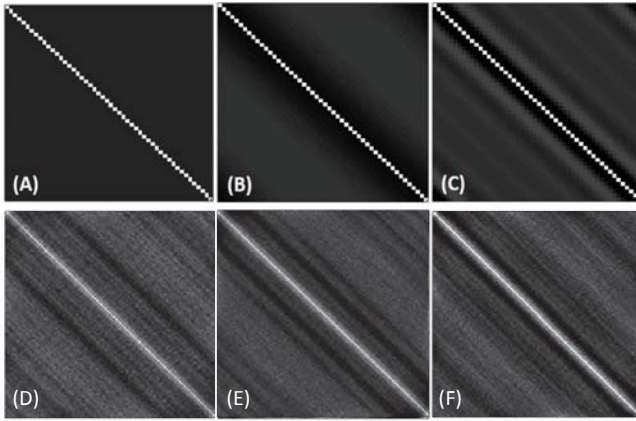for $N \times N$ matrix $\mathbf{1}$ in which every element is set to one.

Fig. 3.   The top row shows 100×100 $\mathbf{Q}_{PD}$ matrices for, respectively, a DC cancellation filter, 12.25 Hz FIR high-pass filter, and 60 Hz FIR high-pass filter. Each matrix in the top row implements the operation of high-pass filtering and summing in the time domain via Eq (7) to yield signal power measurements for conventional PD estimates. The 100×100 matrices (D), (E) and (F) are $\mathbf{Q}$ matrices for the ID estimator (unfiltered echo data) at three perfusion rates, 0.4, 1.0 and 2.0 ml/min, respectively. Each experimentally-measured matrix is the difference between two inverse covariance matrices via Eq (4), and has patterns characteristic of the pair of flow states being compared. The covariance matrices forming $\mathbf{Q}$ in the bottom row are stationary and thus Toeplitz; each was formed using an ensemble of 50,000 packets to obtain low-noise estimates.

F. $\mathbf{Q}_{PD}$ and $\mathbf{Q}$ Matrices

Fig. 3 displays $\mathbf{Q}_{PD}$ (top row) and $\mathbf{Q}$ (bottom row) matrices as images. $\mathbf{Q}_{PD}$ matrices are for the DC cancellation filter (A), a 12.25-Hz high-pass FIR filter (B), and 60-Hz high-pass FIR filter (C). $\mathbf{Q}_{PD}$ are formed independent of echo data because they are simply implementations of high-pass filters.

In contrast $\mathbf{Q}$ are formed from echo signals recorded at specific perfusion states. Parts (D), (E) and (F) show $\mathbf{Q}$ matrices for steady blood-mimicking perfusion at three rates compared with their controls. Because each is the difference between two inverse covariance matrices, it is hard to intuit the patterns in each case. The bottom row shows that $\mathbf{Q}$ matrices describe experimental information specific to the combination of pulse properties, echogenicity and perfusion properties that do not appear in the generic $\mathbf{Q}_{PD}$ of the top row.

G. Discrimination Performance

Performance quantifies the ability to achieve a task. Flow-discrimination performance is measured by comparing AUC values resulting when perfusion estimates are used to differentiate distinct perfusion states.

Fig. 4 illustrates the formation of ROC curves from histograms of $\ell(\mathbf{x}|1)$ for test state 1 (0.4 ml/min blood-mimicking fluid flow) and $\ell(\mathbf{x}|0)$ for control state 0 (0.4 ml/min water flow). The histograms provide estimates of the probability of detection, $P_D = P(\ell(\mathbf{x}|1) > \tau)$, versus the probability of false alarm, $P_F = P(\ell(\mathbf{x}|0) > \tau)$ [21]. That is, $P_D(\tau)$ and $P_F(\tau)$ are found by summing the histograms from $\tau \leq \ell(\mathbf{x}) < \infty$ over all possible τ to generate the ROC curve shown on the right. Perfect detection yields AUC = 1, which occurs when the two distributions do not overlap. A worthless detector generates an AUC = 0.5 that results from the two probability distributions being identical.
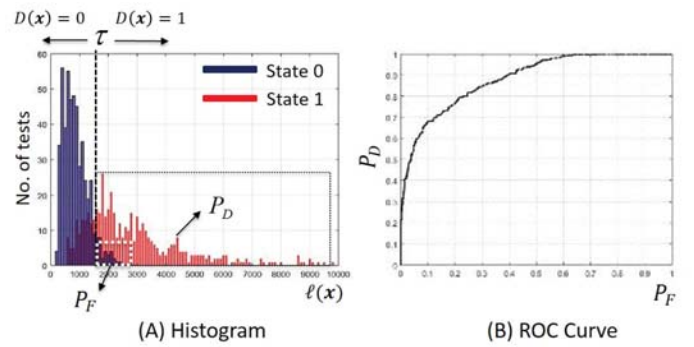

Fig. 4.   (A) Histogram of likelihood ratios ℓ found from phantom measurements for two perfusion states. The distributions of clutter and noise are the same for the two states, but the blood flow states are different. Red and blue histograms represent $\ell(\mathbf{x}|1)$ and $\ell(\mathbf{x}|0)$, respectively. The probability of correctly detecting blood-mimicking fluid perfusion is P_D and the false alarm probability is P_F. These are found by integrating histograms for $\ell(\mathbf{x}|1)$ and $\ell(\mathbf{x}|0)$ above threshold τ. (B) The ROC curve is a plot of P_D versus P_F as discrimination threshold τ is varied. AUC in this case is 0.83.

The efficiency η by which standard power-Doppler techniques distinguish two perfusion states compared to that of the ideal discriminator for the same task is computed using [11]

$$\eta = \frac{\Phi^{-1}(\mathrm{AUC}_{PD})}{\Phi^{-1}(\mathrm{AUC}_{ID})} \,. \tag{9}$$

Function $\Phi^{-1}(\cdot)$ is the inverse of the cumulative normal function, and AUC_{PD} and AUC_{ID} are areas under the ROC curves for the standard power-Doppler and ideal-discriminator approaches, respectively.

H. PCA Filtering

When we know the echo covariance matrix, e.g., if we can precisely measure it for known perfusion conditions, there is no need to separate the different contributions since each known source of covariance becomes part of the ID calculation. Clutter and noise filtering are required clinically because these covariances are unknown. We were concerned that errors made while estimating the covariance matrix might degrade classification performance below the ideal (maximum) value. To address this concern, we studied how the size of the echo-data training set influenced performance and report the results below. During that study, we also asked if filtering the training data used to estimate $\mathbf{\Sigma}_x$ to suppress clutter and noise might allow ideal performance to be achieved with less training data.

This section describes our implementation of principal-components analysis specifically for reducing errors in covariance matrix estimates. Filtering out sources that contribute to $\mathbf{\Sigma}_x$ is a reduction in dimensionality [14], [15], [17]–[19] that we seek to achieved by identifying matrix $\mathbf{W}$ that returns clutter- and noise-suppressed vector $\mathbf{y}$ from training echoes $\mathbf{x}$. That is,

$$\mathbf{y} = \mathbf{W}\mathbf{x} \,, \tag{10}$$

where $\mathbf{x} \in \Re^{N \times 1}$, $\mathbf{y} \in \Re^{J \times 1}$, and $\mathbf{W} \in \Re^{J \times N}$ for $J \leq N$. $\mathbf{W}$ is chosen to maximize the separability of likelihood
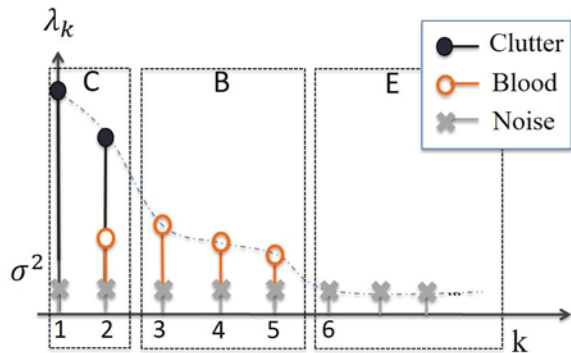
Fig. 5. A simplified eigen-spectrum of Doppler echo-signal vector $\mathbf{x}_m$ where eigenvalues λ_k are sorted in decreasing order. Values are grouped into sets, C, B and E, that approximate the three sources contributing to Σ_x.

functions $p(\mathbf{y}|0) = p(\mathbf{Wx}|0)$ and $p(\mathbf{y}|1) = p(\mathbf{Wx}|1)$ for the two perfusion states; i.e., there is a function f such that

$$\mathbf{W} = \arg\max_{W'} f(p(\mathbf{W'x}|0), p(\mathbf{W'x}|1)) . \quad (11)$$

$\mathbf{W}$ is found from an eigen-decomposition of the covariance matrix

$$\Sigma_{x|i} = \sum_{k=1}^{N} \lambda_k \mathbf{u}_k \mathbf{u}_k^{\mathsf{T}} \quad (12)$$
$$= \sum_{k \in C} \lambda_k \mathbf{u}_k \mathbf{u}_k^{\mathsf{T}} + \sum_{k \in B} \lambda_k \mathbf{u}_k \mathbf{u}_k^{\mathsf{T}} + \sum_{k \in E} \lambda_k \mathbf{u}_k \mathbf{u}_k^{\mathsf{T}} ,$$

where eigenvalues λ_k and eigenvectors $\mathbf{u}_k$ are listed in descending order left to right and grouped into three subspaces C, B and E as shown in Fig. 5.

Moving-tissue echoes (clutter) typically contribute the largest eigenvalues to $\Sigma_{x|i}$, as tissue scattering is more echogenic than blood scattering. Also, the spatially coherent and temporally periodic patterns of clutter motion concentrates its eigenmodes into a low-dimensional subspace with eigenvectors $\{\mathbf{u}_k | k \in C\}$. In contrast, the weaker scattering of red-blood cells generates blood-echo components in lower-amplitude eigenvalues. As perfusion often generates a more diverse pattern of scatterer motion than clutter, it forms a somewhat larger-dimensional subspace with eigenvectors $\{\mathbf{u}_k | k \in B\}$. Acquisition noise is typically the smallest-energy component of the echo-signal covariance and it usually spans the entire basis.

Given that blood components in B correspond to eigenvalues at $\{k, \cdots, k+J-1\}$ ($k = 3, 4, 5$ in the simplified example of Fig. 5), then $\mathbf{y}$ is found from the projection of signal vector $\mathbf{x}$ onto that feature space. In terms of Eq. (10) we have,

$$\mathbf{W} = \left[\mathbf{u}_k, \mathbf{u}_{k+1}, \cdots, \mathbf{u}_{k+J-1}\right]^{\mathsf{T}} . \quad (13)$$

Consequently, J is the cardinality of set B since we assume the other subspaces have no information useful for discriminating perfusion states. In this study, we selected k and J for PCA filtering by discovering which subgroup of eigenvalues maximized flow discrimination performance via AUC measurements.

The eigenbasis cannot completely separate blood and clutter components but, among all orthonormal bases of that dimension, it spans the maximum clutter-signal energy such that the mean-square error between it and the true clutter signal is minimized [22].

Applying PCA filtering to covariance matrix estimates, we have

$$\Sigma_{y|i} = \mathbf{W}_i \Sigma_{x|i} \mathbf{W}_i^{\mathsf{T}} , \qquad i = 0, 1 ,$$
$$\tilde{\ell}(\mathbf{x}) = \mathbf{x}^{\mathsf{T}}(\mathbf{W}_0^{\mathsf{T}} \Sigma_{y|0}^{-1} \mathbf{W}_0 - \mathbf{W}_1^{\mathsf{T}} \Sigma_{y|1}^{-1} \mathbf{W}_1)\mathbf{x}$$
$$= \mathbf{x}^{\mathsf{T}} \tilde{\mathbf{Q}} \mathbf{x} . \quad (14)$$

$\tilde{\mathbf{Q}} \in \Re^{N \times N}$ has rank $J < N$, and so $\tilde{\mathbf{Q}}$ is a reduced-rank version of $\mathbf{Q}$. $\tilde{\mathbf{Q}}$ estimation is illustrated in Fig. 2.

III. RESULTS

A. Data Acquisition

Echo data were recorded using a Sonix RP ultrasonic imaging system (Ultrasonix Medical Corp., Richmond, BC, Canada) and a linear-array transducer. The transducer, located above the dialyzer cartridge, probes the fibers with narrow-band pulses at a Doppler angle of 50 degrees. Tests with blood-mimicking fluid provide perfused-state data including clutter, blood, and noise signals. Control data were recorded by replacing the blood-mimicking fluid with degassed water, thus maintaining the same clutter and noise signal. Table I summarizes the experimental parameters.

TABLE I
ACQUISITION PARAMETERS

Parameter	Value
Probe type	Ultrasonix L14-5
Pulse center frequency	5.0 MHz
Doppler pulse length	4 cycles
In-plane transmit focal length	15.75 mm
In-plane transmit f-number	2.02
Testing ensemble size	40-100 pulses
Fractional bandwidth	20%
Axial range of sample volume	2 mm
Pulse repetition frequency	220-650 Hz
Fast-time sampling rate	20 MHz
PD line density (Fig. 10)	2.5/mm

B. Experimental Overview

We compared blood-mimicking fluid perfusion state 1 to its water-only control state 0 to study perfusion *detection* in Experiment I. We then compared two different blood-mimicking perfusion states between 0-2 ml/min to study perfusion *discrimination* in Experiment II. From histograms of test statistic responses, e.g., Fig. 4, AUC values were computed for conventional power Doppler and ID estimators and applied to Eq. (9) to determine estimator efficiency.

Test statistics reported as conventional power-Doppler estimates were computed using Eq. (7). Estimates involved echo data for which either a DC cancellation filter, Eq. (8), or a high-pass FIR filter was applied. Ideal discriminator (ID) test statistics were computed using echo data that was unfiltered via Eq. (4) or PCA-filtered via Eq. (14). We will show in
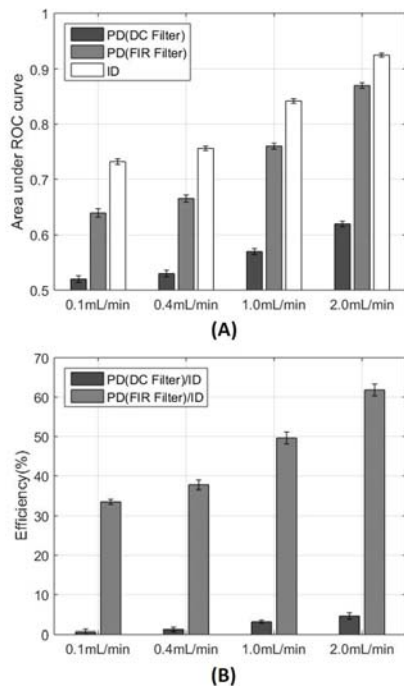
Fig. 6. (A) Areas under ROC curves (AUCs) for perfusion detection using different perfusion rates and estimators. The state 0 condition uses water in place of the blood-mimicking fluid. The white bar indicates ideal-discriminator (ID) performance, and the gray bars are the performances of the conventional power-Doppler (PD) estimator for the DC cancellation and FIR clutter filters. (B) Detection efficiency of Doppler methods relative to the ID method. Error bars denote ± 2 standard errors for 300 trials.
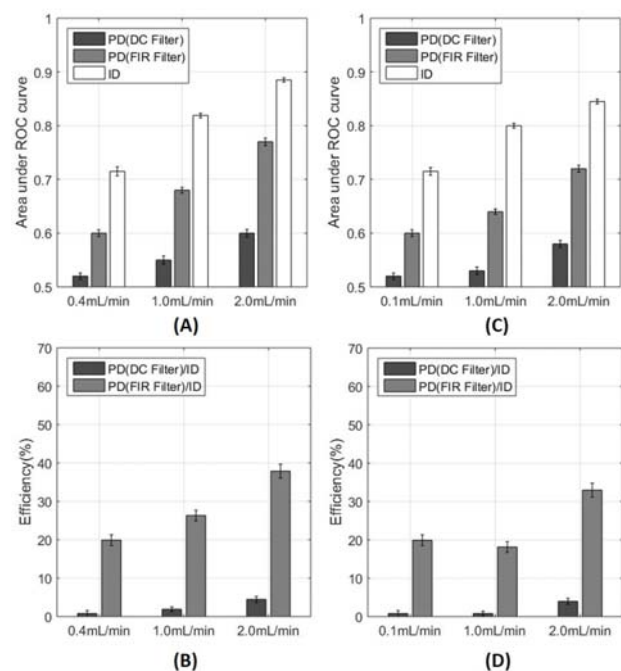

Fig. 7. (A) Areas under ROC curves (AUCs) for perfusion discrimination using different perfusion rates and estimators. In (A) and (B), state 0 applies blood-mimicking fluid perfusion at a rate of 0.1 ml/min while (C) and (D) use state 0 blood-mimicking fluid perfusion at a rate of 0.4 ml/mi. The white bar indicates performance of the ideal-discriminator (ID), and the gray bars are that for the conventional power-Doppler (PD) estimator for the DC cancellation and FIR clutter filters. Results at 0.4 ml/min in (A) and (B) are by definition the same as those at 0.1 ml/min in (C) and (D). Error bars denote ± 2 standard errors for 300 trials.

Experiment IV that the only effect PCA filtering has on ID estimator performance is to improve estimation accuracy with a smaller training set. Experiment V illustrates how the ID formalism can be adapted for imaging under the special situation where the covariances are known.

C. Experiment I: Detection

Experiment I provided data to compare perfusion-detection performances of standard power-Doppler and ideal-discriminator approaches. In each case blood-mimicking fluid perfusion measurements were compared to water-perfused control measurements. Σ_x was estimated using a training set of 3000 vectors each of packet size 100 recorded at PRF = 650 Hz.

Detection performance is summarized in Fig. 6, where testing sets are composed of 300 echo-signal vectors. Doppler estimator results involved an FIR filter having a high-pass corner frequency that was selected to maximize AUC. Fig. 6 (A) shows AUC values for the range of perfusion rates tested relative to the corresponding control state. As expected, performance for each estimator improves as flow rates increase because of better separation between the clutter and blood components. Detection performance estimated from power-Doppler versus ideal-discriminator test statistics is summarized by the efficiency measurements shown in Fig. 6 (B). At flows below 1 ml/min, PD estimators are less than 50% efficient.

D. Experiment II: Discrimination

Experiment II estimated the efficiency for perfusion discrimination of PD estimators. Here we measured the ability of power-Doppler method to *discriminate* various perfusion rates when compared to perfusion at 0.1 ml/min in Fig. 7 (A) and (B). Comparisons are also made relative to 0.4 ml/min in Fig. 7 (C) and (D). Discriminating two perfusion states is more challenging than detection, as quantified by the lower AUC values in Fig. 7 (A) and (C) relative those in Fig. 6 (A). Along with lower overall AUC values, we find that PD estimators are also less efficient at discrimination than detection.

E. Experiment III: PRF and Frequency Resolution

We expect the pulse-repetition frequency (PRF) to have a different influence on perfusion-detection performance than it does on arterial-flow estimation since aliasing is not a limiting factor in perfusion estimation. For perfusion estimation, the total time spanned by packet samples is very influential because it determines the frequency resolution of a Fourier basis. Conditions that improve frequency resolution also increased the number of samples in the B eigen-subspace, which improves perfusion discrimination.

Fig. 8 shows the results of two experiments that demonstrate the value of high-frequency resolution. In (a), we increase the packet size by increasing PRF without changing the total duration of slow-time measurements to find no measurable
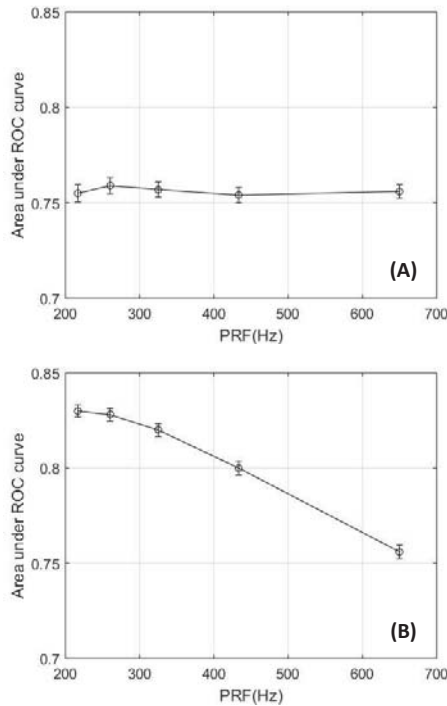
Fig. 8. Plots of detection AUC at 0.4 ml/min perfusion measured from the ID test statistic as a function of pulse-repetition frequency (PRF). In (A), the total time duration of the echo vector is fixed at 0.1864 s and the vector size varies as 0.1538×PRF pulses. In (B), the vector size is fixed at 100 pulses while time duration varies as 100/PRF s. Error bars denote ±2 standard errors for 300 trials.

change in ID detection performance. Conversely, in Fig. 8(b) we fix the packet size at 100 and allow the increase in PRF to decrease the total duration spanned by the packet. We find performance decreases with the reduction in frequency resolution. The change in AUC between PRF = 217 Hz (0.83) and 650 Hz (0.76) is modest, but the corresponding change in efficiency via Eq. 9 is a factor of 2, which is highly significant. The best performance for perfusion detection and discrimination is found at a PRF less than 1kHz and the largest packet size that preserves signal ergodicity.

F. Experiment IV: Effects of PCA Filtering

Fig. 9 illustrates how the number of echo vectors used to estimate the covariance matrix influences ID performance with and without PCA filtering of the training set. In Fig. 9(a), where we used a packet size of 50 pulses, a plateau is reached near AUC $\simeq 0.65$. We only need 400 training vectors to achieve ideal-discriminator performance because the AUC does not increase using a larger number of training vectors. In the plateau region, PCA filtering has no influence on AUC. However, as the number of training vectors falls below 400, we find AUC also falls as errors in covariance estimates increase; below 400 training vectors, we are not estimating the ideal-discriminator response. We see that the reduction in AUC values below 400 vectors is less using PCA-filtered echo signals to estimate Σ_x because we generate fewer covariance errors by suppressing the clutter and noise components.
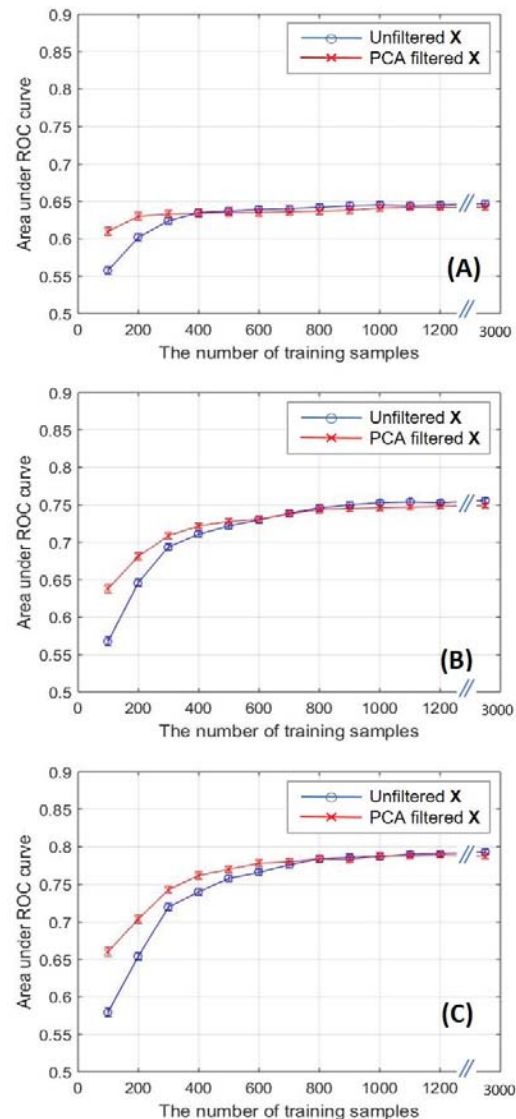

Fig. 9. Changes in detection AUC at 0.4 ml/min as a function of the number of vectors used to estimate the covariance matrices (training samples) and test-vector length (packet size). Test-vector sizes are (A) 50, (B) 100, and (C) 150 pulses. Points marked (o) are for the ID estimator in which the echoes used to estimate covariance were unfiltered. Points marked (x) use PCA-filtered echo signals. Note that the point at the far right in each plot is for 3000 training vectors. Error bars denote ±2 standard errors for 300 trials.

Increasing the test vector packet size to 100 in Fig. 9(b) and to 150 in Fig. 9(c) at fixed PRF raises the detection-performance plateau because of increased in frequency resolution. However, we must increase the training set to 800 vectors or more before a plateau is reached.

The data of Fig. 9 show that ID performance is not affected by echo-data filtering, although PCA-filtering generates fewer covariance estimation errors leading to performance estimates closer to the ideal discriminator. It also provides evidence that clutter filtering is not fundamental to achieving optimal discriminability when statistical properties of the echo signal are known or can be measured; the need for clutter filtering depends on the requirements of the perfusion estimator adopted.

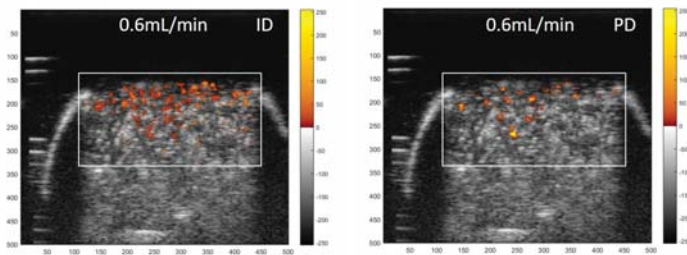The following computational times were measured using

Fig. 10. Conventional power-Doppler image of phantom perfusion at 0.6 ml/min (right) and that obtained using the ID estimator (left) for the same recorded echo data. Results are coded in color and overlaid on the B-mode image. The image is a cross sectional view of the dialyzer cartridge diagrammed in Fig. 1.

an Intel processor i5-4300U CPU, 2.50GHz running MATLAB 2013b. The average time to compute $\mathbf{Q}$ matrices (training) was 0.028s without PCA filtering and 0.106s with PCA filtering. The computational time for testing was 0.068s per data set.

G. Experiment V: Imaging

We illustrate in Fig. 10 the effects of lower detection efficiency by comparing standard Doppler estimation with a statistical estimator inspired by the ID approach. Note that this method is only possible because we have training sets of known perfusion rates.

Perfusion was estimated for the phantom of Fig. 1 by extending Eq. (4) to M-ary hypothesis testing using

$$\ell_k(\mathbf{x}) = \ln \frac{p(\mathbf{x}|k)}{p(\mathbf{x}|0)} \simeq d_k + \mathbf{x}^\top \mathbf{Q}_k \mathbf{x} \,, \qquad (15)$$

where $d_k = \log(|\mathbf{\Sigma}_{x|0}|/|\mathbf{\Sigma}_{x|k}|)$ is the logarithm of the ratio of deteriminants, $\mathbf{Q}_k = \mathbf{\Sigma}_{x|0}^{-1} - \mathbf{\Sigma}_{x|k}^{-1}$ and $k \in \{1, 2, \cdots, 19, 20\}$ denotes the 20 nonzero perfusion states between 0.1 and 2.0 ml/min for which covariances were estimated. The perfusion estimate at each location is found from $\mathbf{Q}_k$ that maximizes the test statistic,

$$D(\mathbf{x}) = \arg \min_k (\ell_k(\mathbf{x})) \,. \qquad (16)$$

The procedure for estimating the covariance matrices is the same as that in Section II-D. Then we estimated $\ell_k(\mathbf{x})$ for all the test data in the 2-D spatial window shown in Fig. 10. Test vectors consist of 40 (200 Hz × 0.2 s) slow-time echo signals at each window position over a 400-sample axial range ((15.4 mm × 20 samples/μs)/(0.77 mm/μs)=400 samples) and a 65 scan line lateral range ((25.8 mm)/(0.4 mm/scanline) = 65 scan lines). The total number of test vectors is 400×65, one for each point in the white box of Fig. 1, and each test vector has 40 samples. The image on the left side of Fig. 10 was obtained by color coding the results of the test vector by Eq. (16) at each pixel according to the twenty flow states possible and superimposing those values on the B-mode image. A conventional Doppler image with the same color mapping is shown on the right.

IV. DISCUSSION

The efficiency of conventional power-Doppler methods using FIR clutter filtering for detecting and discriminating perfusion-like blood velocities without contrast enhancement is in the range of 20-50%. This finding suggests there may be more efficient label-free perfusion estimators. Examining Eq. (4) we see that the strategy of the ideal discriminator is to use the entire covariance matrix in decision making, which is only possible if the states being compared are known statistically. Each echo covariance matrix is a specific combination of properties of the interrogating pulse and scatterer reflectivity and motion. Conventional power Doppler methods do not apply the covariance matrix during the power calculation, which means they sub-optimally weight echo signals during the squaring and summing process.

Perfusion images are enhanced to reveal flows that are closer to the true value by properly weighting each test vector with covariance information. We demonstrated enhanced flow in the phantom via the image of Fig. 10, however, this approach is only possible when the true covariance estimate can be accurately estimated for a known flow condition. Future work includes development of statistical flow estimators that introduce covariance matrix information into process. Even if the method is sub-optimal, independently validated in vivo testing will be able to quantify benefits. Importantly, the methods described in this paper can be applied to any new estimator to measure its discrimination efficiency and be compare those results with standard approaches to evaluate efficacy.

There are two further issue with respect to our study to note. The high attenuation of the dialyzer cartridge fibers reduces the echo SNR because of greater attenuation and less penetration. Also we assumed spectrally white acquisition noise in Eq. (1) despite there being a slight reduction in the noise spectrum ($\sim$1.6 dB) from zero frequency to Nyquist (red-shifted noise). Nevertheless, both conditions apply equally to $\ell(\mathbf{x})$ for ID and PD methods and therefore estimator efficiency is not affected. For the same reasons, we expect the efficiency of discrimination for superficial and deep tumors to be roughly equivalent even though the performance for detecting perfusion in deep tumors is lower than for superficial tumors.

REFERENCES

[1] J. Rubin, R. Bude, P. Carson, R. Bree, and R. Adler, "Power Doppler US: a potentially useful alternative to mean frequency-based color Doppler US," *Radiology*, vol. 190, no. 3, pp. 853–856, 1994.
[2] M. Walther, H. Harms, V. Krenn, S. Radke, S. Krischner, and F. Gohlke, "Synovial tissue of the hip at power Doppler US: correlation between vascularity and power Doppler US signal," *Radiology*, vol. 225, no. 1, pp. 225–231, 2002.
[3] W. Yang and P. Dempsey, "Diagnostic breast ultrasound: current status and future directions," *Radiol Clin North Am*, vol. 45, no. 5, pp. 845–861, 2007.
[4] N. Oebisu, M. Hoshi, M. Ieguchi, J. Takada, T. Iwai, M. Ohsawa, and H. Nakamura, "Contrast-enhanced color Doppler ultrasonography increases diagnostic accuracy for soft tissue tumors," *Oncol Rep*, vol. 32, no. 4, pp. 1654–1660, 2014.

[5] A. Broumas, R. Pollard, S. Bloch, E. Wisner, S. Griffey, and K. Ferrara, "Contrast-enhanced computed tomography and ultrasound for the evaluation of tumor blood flow," *Invest Radiol*, vol. 40, no. 3, pp. 134–147, 2005.

[6] M. Hwang, K. Niermann, A. Lyshchik, and A. Fleischer, "Sonographic assessment of tumor response: from in vivo models to clinical applications," *Ultrasound Quarterly*, vol. 25, no. 4, pp. 175–183, 2009.

[7] P. A. Dijkmans, C. Visser, and O. Kamp, "Adverse reactions to ultrasound contrast agents: Is the risk worth the benefit?" *Euro J Echocard*, vol. 6, no. 5, pp. 363–366, 2005.

[8] J. Hanley and B. McNeil, "The meaning and use of the area under the receiver operating characteristic (ROC) curve," *Radiology*, vol. 143, no. 1, pp. 29–36, 1982.

[9] R. Zemp, C. Abbey, and M. Insana, "Ideal observer model for detection of blood perfusion and flow using ultrasound," *Inf Process Med Imaging*, vol. 18, pp. 318–329, 2003.

[10] H. Barrett and K. Myers, *Foundations of Image Science*. Hoboken NJ: Wiley-Interscience, 2004.

[11] C. Abbey, R. Zemp, J. Liu, K. Lindfors, and M. Insana, "Observer efficiency in discrimination tasks simulating malignant and benign breast lesions imaged with ultrasound," *IEEE Trans Med Imag*, vol. 25, no. 2, pp. 198–209, 2006.

[12] A. Heimdal and H. Torp, "Dectecting small blood vessels in color flow imaging: a statistical approach," *IEEE Proc Ultrason Symp*, pp. 1219 – 1222, 1997.

[13] S. Hovda, H. Rue, and B. Olstad, "New Doppler-based imaging method in echocardiography with applications in blood/tissue segmentation," *Med Imag Informatics*, vol. LNCS-4987, pp. 207–215, 2008.

[14] I. Jolliffe, *Principal component analysis*. New York: Springer, 2002.

[15] C. Gallippi and G. Trahey, "Adaptive clutter filtering via blind source separation for two-dimensional ultrasonic blood velocity measurement," *Ultrasonic Imaging*, vol. 24, no. 4, pp. 193–214, 2002.

[16] In vivo perfusion is the steady-state delivery of blood to a unit of tissue, often measured in units of flow per tissue mass. For example, reported perfusion measurements in VX2 rabbit tumors spans a large range, from 13.5 ml/min/100 g using PET techniques [23] to 0.2-1.1 ml/min/g using radioactive microspheres [24]. In this report, *perfusion* is the directed flow of blood-mimicking fluid through a fixed $\sim 2 \text{cm}^2$ cross sectional area of 25-cm-long packed microtubules; the total flow is varied between 0.1-2.0 ml/min.

[17] A. C. Yu and R. S. Cobbold, "Single-ensemble-based eigen-processing methods for color flow imaging–part ii. the matrix pencil estimator," *IEEE Trans Ultrason Ferroelectr Freq Control*, vol. 55, no. 3, pp. 573–587, 2008.

[18] A. Yu and L. Lovstakken, "Eigen-based clutter filter design for ultrasound color flow imaging: a review," *IEEE Trans Ultrason Ferroelectr Freq Control*, vol. 57, no. 5, pp. 1096–1111, 2010.

[19] C. Demene, T. Deffieux, M. Pernot, B. F. Osmanski, V. Biran, J. L. Gennisson, L.-A. Sieu, A. Bergel, S. Franqui, J. M. Correas, I. Cohen, O. Baud, and M. Tanter, "Spatiotemporal clutter filtering of ultrafast ultrasound data highly increases Doppler and fUltrasound sensitivity," *IEEE Trans Med Imag*, vol. 34, no. 11, pp. 2271–2285, 2015.

[20] H. van Trees, *Detection, Estimation, and Modulation Theory, Part I*. John Wiley and Sons, NY, 1968.

[21] N. Nguyen, C. Abbey, and M. Insana, "Objective accessment of sonographic quality I: Task information," *IEEE Trans Med Imag*, vol. 32, no. 4, pp. 683–690, 2103.

[22] S. Bjærum, H. Torp, and K. Kristoffersen, "Clutter filters adapted to tissue motion in ultrasound color flow imaging," *IEEE Trans Ultrason Ferroelectr Freq Control*, vol. 49, no. 6, pp. 693–704, 2002.

[23] S. Cherry, P. Carnochan, J. Babich, F. Serafini, N. Rowell, and I. Watson, "Quantitative in vivo measurements of tumor perfusion using rubidium-81 and positron emission tomography," *J Nucl Med*, vol. 31, no. 8, pp. 1307–1315, 1990.

[24] R. Jain and K. Ward-Hartley, "Tumor blood flowcharacterization, modifications, and role in hyperthermia," *IEEE Trans Son Ultrason*, vol. 31, no. 5, pp. 504–529, 1984.

MinWoo Kim received his B.S. and M.S. degrees in the Department of Bio and Brain Engineering from Korea Advanced Institute of Science and Technology (KAIST) in 2007 and 2009, respectively. From 2009 to 2012, he was a research engineer at Samsung Medison Co., Ltd. specializing in ultrasonic imaging equipment. He is currently a Ph.D. candidate in the Department of Electrical and Computer Engineering at the University of Illinois at Urbana-Champaign. His research is on blood perfusion imaging to detect cancers using ultrasonic signal processing.

Craig K. Abbey received his PhD in applied mathematics from the University of Arizona in 1998. He was a postdoctoral fellow in medical physics at Cedars-Sinai Medical Center and UCLA from 1998 to 2001. From 2001 to 2004 he was a member of the faculty in biomedical engineering at UC Davis. His primary affiliation is in the Dept. of Psychological and Brain Sciences at UC Santa Barbara. His research focuses on the transfer of diagnostic information in medical imaging systems utilizing theoretical analysis of image statistics as well as visual psychophysics for evaluating human observer performance.

Michael F. Insana received his PhD in medical physics from the University of Wisconsin Madison in 1983. He is currently Willett Professor of Engineering and a faculty member in the Departments Bioengineering and ECE at the University of Illinois at Urbana-Champaign. He also leads the Bioimaging Science and Technology group at the Beckman Institute on campus. He was the Head of the Department of Bioengineering in its early years from 2008-2013. Michael is a Fellow of the IEEE, Acoustical Society of America, Institute of Physics, and American Institute of Medical and Biological Engineering. He is currently Editor-in-Chief of the IEEE Transaction on Medical Imaging.